# Three-Dimensional Investigation of Wave-Pile Group Interaction Using the Scaled Boundary Finite Element Method

## Part I: Theoretical Developments

Miao Li[a,*], Hong Zhang[a], Hong Guan[a] and Gao Lin[b]

[a] Griffith School of Engineering, Griffith University, *QLD*, 4222, Australia

[b] Faculty of Infrastructure Engineering, Dalian University of Technology, Dalian, 116024, China

*Corresponding author. Tel: +61 7 555 27608. Email address: m.li@griffith.edu.au

ABSTRACT

In this study, the three-dimensional wave-pile group interaction mechanism is investigated by addressing both wave behaviour and pile group responses. The Scaled Boundary Finite Element Method (SBFEM) is employed to develop the computational model. This paper, Part I of the study, mainly focuses on the theoretical development of the problem. A SBFEM model is developed to formulate both equations governing the wave motion and the structural behaviour. The proposed model, with its accuracy verified by wave interaction with a single pile foundation, is capable of addressing wave interaction with any arbitrary number of piles with various cross-sections and spatial

layouts.

KEY WORDS: wave-pile group interaction; diffraction; structural behaviour; scaled boundary finite element method; three dimensions

## 1. INTRODUCTION

Pile foundations are one of the most commonly used foundation structures for coastal and offshore installations, such as oil-drilling platforms, offshore airports and wind farms. They are also extensively used in ports and harbour areas in the form of piers for bridges or jetties for mooring. Normally, piles appear in clusters, i.e. a group of piles are arranged in specific layouts and separated by certain distances to provide enhanced functional ability. One significant difference between pile foundations designed for ocean constructions and those for onshore installations lies in the surrounding environment to which they are subjected and accordingly the external forces they have to withstand. By exerting constant and detrimental forces onto structures, waves are the most significant environmental concern, and therefore the main consideration for designing and maintaining ocean structures (Benassai, 2006; Goda, 2010). Investigations of engineering failures have established that waves can be a critical factor causing accidents in ocean installations (U.S. Coast Guard, 1983; Moan, 2005). Therefore, the analyses of waves, i.e. their behaviour in the presence of, and their impact on pile group foundations, and the

corresponding pile group's performance are of vital importance for safe and reliable design, and optimal usage of pile group foundations.

Significant research has been carried out by ocean engineers focusing on wave behaviour in the presence of, and the corresponding wave forces exerted on multiple vertical cylinders. Spring and Monkmeyer (1974) analytically formulated the first-order plane wave forces on groups of two bottom-fixed, surface-piercing vertical cylinders. Linton and Evans (1990) simplified the theory proposed by Spring and Monkmeyer (1974) and investigated the first-order diffraction problem of a regular incident wave in the presence of $N$ bottom-mounted vertical circular cylinders. An important breakthrough can be identified as the generalised wave-structure interaction theory derived by Kagemoto and Yue (1986), which is applicable to arrays of arbitrary structures with two specifications: (1) the vertical projections of the structures on a horizontal plane cannot overlap with each other; and (2) fictitiously introduced circles on the projection plane to enclose individual structures cannot enclose centres of other circles. Yilmaz and Incecik (1998) employed Kagemoto and Yue's (1986) formulation to address wave diffraction by a group of truncated vertical cylinders. The mushrooming of very large floating structures supported by thousands of cylindrical legs led to the work of Maniar and Newman (1997) and Kashiwagi (2000). They employed a hierarchical procedure to first divide the entire

cylinder group into small clusters. These clusters were later assembled to build up the whole array.

Recently, Walker and Eatock Taylor (2005) extended the linear diffraction theory to 'NewWaves' interaction with linear array of cylinders. Wang and Wu (2007) investigated the second-order wave diffraction problem with an array of vertical cylinders in the time domain, capturing the transient effect when the wave motion is not periodic. Zhao *et al.* (2008) examined the wave diffraction by an array of truncated cylinders. Chatjigeorgiou and Mavrakos (2010) derived a semi-analytical formulation, using Mathieu functions in the elliptic coordinate system, for wave diffraction with an array of elliptical cylinders. Tao *et al.* (2009) studied the wave field behaviour in the presence of two adjacent square caissons. Song *et al.* (2010) further extended the wave diffraction problem to multiple cylinders of arbitrary cross-sections.

It is found that intensive effort has been directed towards the wave analysis to investigate wave parameters due to the influence of structures, such as the free surface elevation, wave propagation velocity and the hydrodynamic pressure. These studies provide explicit wave data for subsequent structural analyses. However, they are normally formulated in certain situations for specific applications. The Morison equation is effective when the structure's influence on wave transformation is negligible. The formula proposed in Zhu

(1993) is only applicable to circular cylinders subjected to short-crested waves. In other cases concerning complexity, the linkage between the two processes becomes challenging. For an effective evaluation of the structural behaviour, an investigation involving both waves and structures needs to be performed.

However, due to the dissimilar physical nature as found in waves and structures, the study in this aspect has not yet been adequately documented. Waves exist in an extensive domain, and their behaviour is governed by scalar equations, normally with the velocity potential as the unknown variable. Structures, on the other hand, are characterised by finite dimensions, and their behaviour is described by vector equations addressing displacements and stresses. These differences in the theoretical background between wave and structural analyses impede the compiling of an integrated wave-structure interaction model. In this regard, a few documented studies (Lee and Wang, 2000; Wu et al., 1995) set a precedent. However, these studies were mostly conducted in two dimensions, and the boundary conditions associated with the wave analysis were not treated properly. This is directly or indirectly restricted by the time consumption and memory requirement involved in three-dimensional analyses. Moreover, the methodology employed in the analysis can also be a reason for this restriction. The complex nature of the interaction problem, together with other issues such as the unbounded scope of the

study domain and the dissimilar nature of the multi-physical field, precludes the acquisition of an analytical solution or an experimental investigation. The Finite Element Method (FEM), though possessing numerous advantages such as the flexibility when dealing with inhomogeneous and anisotropic materials, runs into difficulties when unbounded domains are involved. The Boundary Element Method (BEM), though well suited to model unbounded domains, needs to evaluate singular integrals and suffers from irregular frequencies. These disadvantages render them inappropriate to be employed in the wave-pile group interaction analysis specified in this study.

Encouragingly, the Scaled Boundary Finite Element Method (SBFEM), originally developed to address wave propagation problems within the framework of dynamic unbounded medium-structure interaction (Song and Wolf, 1997; Wolf and Song, 1996), overcomes the drawbacks mentioned above and has been applied to solve many problems in fracture mechanics (Yang, 2006; Yang and Deeks, 2007), computational electromagnetics (Liu et al., 2010), geotechnical engineering (Bazyar, 2007) and hydraulic engineering (Wang et al., 2010). It also has been employed to address wave diffraction problems around breakwaters and caissons (Li, 2007; Tao et al., 2007). Studies show that SBFEM has demonstrated high efficiency and accuracy in solving wave domains when waves interact with structures. Contrary to FEM, domain truncations

and artificial boundary conditions do not need to be treated in situations with unbounded computational domain; Unlike BEM, fundamental solutions and singular integral evaluations are not required, and numerical difficulties associated with irregular frequency and sharp corners do not need to be addressed. This, spontaneously and inspiringly, provokes the motivation of utilising SBFEM to solve the wave-pile group interaction problem, investigating both the wave motion in the presence of pile groups and pile groups' reaction subjected to wave forces.

Most recently, Li *et al*. (2010b; 2011) used SBFEM to study the structural behaviour of offshore monopiles when subjected to ocean wave loads. In Li *et al*. (2010b; 2011), the analytical wave formula in Zhu (1993) was employed, and only the equations governing the monopile's behaviour was formulated in the SBFEM model. The present study is an enhanced development of the previous work. Both the wave field and the pile group are incorporated in an integrated SBFEM model. As Part I of this study, this paper presents the theoretical formulation. The wave field behaviour and the pile group response are described mathematically in Section 2. The SBFEM model is constructed in Section 3 with a detailed solution proposal, which is verified in Section 4 by wave interaction with a single pile foundation. Finally, the paper concludes by summarising significant contributions in Section 5. The numerical results of wave interaction with pile group

foundations will be discussed in an accompanying paper as Part II of this study.

## 2. PROBLEM FORMULATION

A group of pile foundations in an ocean environment subjected to ocean wave forces are illustrated in Fig. 1. The piles are assumed to be fixed at the seabed surface and the relative motion between the piles and the seabed is neglected. In addition, external loads from superstructures, not being the main focus of this study, are not addressed in the current discussion. The origin $O$ of the Cartesian coordinate system is located at the seabed surface. $x$ and $y$ denote two orthogonal horizontal directions, and $z$ positively points upwards. Here, $\Omega$ represents the field with sea water. $A$ denotes the wave amplitude; $d$ the mean water depth. $a$ and $h$ represent the radius and the height of the pile foundation, respectively.

### *2.1. Wave field behaviour*

Under the assumption that the flow motion is irrotational, and that the fluid is invisid and incompressible, the velocity potential $\Phi$ of the wave field $\Omega$ is governed by the Laplace equation (Mei, 1989):

$$\nabla^2 \Phi = 0 \text{ in } \Omega \tag{1}$$

The concept of separation variables is employed to decompose $\Phi$ into univariate

functions with respect to the independent variables, i.e. the spatial variables $x$, $y$, and $z$, and the temporal variable $t$:

$$\Phi(x, y, z, t) = \phi(x, y)\, Z(z)\, e^{-i\omega t} \tag{2}$$

In Eq. (2), $Z(z)$ is formulated as:

$$Z(z) = \frac{\cosh kz}{\cosh kd} \tag{3}$$

to account for the boundary condition that no flow across the seabed surface. The linearised free surface boundary condition is satisfied by the dispersion relation. Substituting Eq. (2) into Eq. (1) leads to a Helmholtz equation governing the wave motion at the free surface level two-dimensionally:

$$\nabla^2\phi + k^2\phi = 0 \tag{4}$$

It should be mentioned that $\Phi$ and $\phi$ in Eqs. (1), (2) and (4) represent any of the total (denoted by a subscript '$T$'), the incident (denoted by a subscript '$I$') and the scattered (denoted by a subscript '$S$') velocity potentials.

The Neumann boundary condition and the Sommerfeld radiation condition (Sommerfeld, 1949) are specified respectively as:

$$\phi_{T,n} = 0 \quad \text{at the wetted structure face} \tag{5}$$

and

$$\lim_{kr\to\infty} (kr)^{1/2} \left(\phi_{S,r} - ik\phi_S\right) = 0 \ \text{ at infinity} \tag{6}$$

Therefore, by introducing Eqs. (2) and (3), a three-dimensional wave diffraction problem described by Eq. (1) is spatially reduced to a two-dimensional problem governed by Eq. (4), subjected to Eqs. (5) and (6).

*2.2. Structural response*

The structural behaviour of the pile group foundation is governed by the elasto-static differential equation (Gould, 1994):

$$[L]^T \{\sigma\} = 0 \tag{7}$$

with [$L$] being the partial differential operator. The stress amplitude {$\sigma$} is related to the strain amplitude {$\varepsilon$} and the elastic matrix [$D$] as:

$$\{\sigma\} = [D]\{\varepsilon\} \tag{8}$$

The strain amplitude {$\varepsilon$} and displacement amplitude {$u$} are related by [$L$] in the form of:

$$\{\varepsilon\} = [L]\{u\} \tag{9}$$

The structural behaviour of each pile subjected to external wave forces is to be investigated three dimensionally with the boundary condition specified at the seabed level.

## 3. SBFEM MODEL AND SOLUTION PROCEDURE

SBFEM is a semi-analytical numerical method proposed in mid-1990s (Song and Wolf, 1996a, 1996b, 1997). Its concept of solving problems originates from the Finite Element Method (FEM) and the Boundary Element Method (BEM). It inherits the idea of discretisation and interpolation from FEM, but only along the boundary as in BEM, which reduces the spatial dimension of the problem by one, and significantly minimises the discretisation effort and leads to a substantially reduced number of degrees of freedom. Fundamental solutions are not required, as would be the case in BEM. Boundary conditions at infinity for problems involving unbounded domains can be exactly satisfied. Despite some disadvantages when dealing with problems involving nonlinearity and material inhomogeneity, SBFEM is well-suited to address the wave-structure interaction problem specified in this study. This will be demonstrated in Sections 3.1 and 3.2 by illustrating SBFEM formulations of the wave and the structural analyses, respectively.

*3.1. Wave domain formulation*

As discussed in Section 2.1, the wave diffraction due to the presence of pile groups in three dimensions governed by Eq. (1) has been transformed to a problem addressed by the Helmholtz Eq. (4) two dimensionally at the free surface level. The *xy* plane view of an infinite wave domain and a group of pile foundations is illustrated in Fig. 2, where the number of piles is arbitrarily chosen as three (denoted by P1, P2 and P3), and the piles are of circular cross-sections with a randomly arranged spatial layout. An auxiliary circular envelope, represented by the dashed line, is introduced to divide the entire wave domain into two: one unbounded domain $S_\infty$ extending from the circular envelope towards infinity, and one bounded domain $S_\mathrm{b}$ within the envelope enclosing the pile group. Before introducing the local scaled boundary coordinate system, a further division of $S_\mathrm{b}$ is performed to meet the requirement that for each subdivided domain, any position on the domain boundary can be visible from a specific location, namely the scaling centre. The subdomain division in SBFEM does not follow any particularly defined standard. It is subjected to the complexity of the boundaries and interfaces involved in the geometric model, i.e. the cross-section and the plane layout of the pile foundations in this study. Generally, subdomains with relatively uniform shapes are favoured. This is similar to the discretisation concept in FEM, where severely distorted polygons (elements) with rather sharp angles are avoided. The location of the scaling centre can theoretically be anywhere

inside the domain, as long as the visibility of the domain boundary from the scaling centre is guaranteed. However, a location allowing for well-balanced distances from the scaling centre to the domain boundary is preferable. It is therefore suggested the scaling centre be positioned at the geometric centre of the corresponding subdomain, to eliminate any possible numerical inaccuracy also benefit the pre-process of the SBFEM calculation. Thus, illustrated in Fig. 2, the entire wave field is discretised into eight subdomains, with seven bounded subdomains $S_i$ ($i$ = 1, 2, …, 7) inside the circular envelope separated by solid lines and one outer unbounded subdomain $S_\infty$ extending to infinity.

A local scaled boundary coordinate system, taking subdomain *S4* for example, is constructed in Fig. 3 (a) by a scaling centre $O$ ($x_0$, $y_0$) and a defining curve $S$, i.e. the boundary of *S4*. Scaling the defining curve $S$ according to a radial coordinate $\xi$ with respect to $O$ leads to a bounded domain (*S4* in this case) when $\xi$ runs from $\xi_0 = 0$ at the scaling centre $O$ to $\xi_1 = 1$ at the defining curve $S$, or alternatively as shown in Fig. 3 (b), the scaling leads to an unbounded domain $S_\infty$ when $\xi$ goes from $\xi_0 = 1$ at $S$ to $\xi_1 = \infty$ at infinity.

In the SBFEM descretisation, only the defining curve needs to be discretised. The local scaled boundary coordinate system ($\xi$, $s$) is related to the Cartesian coordinate system $(\hat{x}, \hat{y})$ as:

$$\begin{aligned}\hat{x}(\xi,s) &= \xi\left[N(s)\right]\{x\} + x_0 \\ \hat{y}(\xi,s) &= \xi\left[N(s)\right]\{y\} + y_0\end{aligned} \tag{10}$$

where $\{x\}$ and $\{y\}$ represent the coordinates of the discretised nodes on $S$; $[N(s)]$ is the geometric mapping function. Note that the coordinate of the Cartesian coordinate space is represented by $(\hat{x}, \hat{y})$ as $(x, y)$ is reserved for the coordinates on the boundary, which is a convention in SBFEM. However, $x$ and $y$ (or $x$, $y$ and $z$) are still used when indicating directions in the following discussions.

With this geometric mapping, the gradient operator $\nabla$ is reformulated in the scaled boundary coordinate system using $\xi$ and $s$ as:

$$\nabla = \left[b^1(s)\right]\frac{\partial}{\partial\xi} + \frac{1}{\xi}\left[b^2(s)\right]\frac{\partial}{\partial s} \tag{11}$$

in which, $[b^1(s)]$ and $[b^2(s)]$ only depend on the boundary discretisation on $S$, and are independent of the radial coordinate $\xi$. Using the same shape function $[N(s)]$ as for the boundary discretisation, the velocity potential $\phi$ is expressed as:

$$\left\{\phi(\xi,s)\right\} = \left[N(s)\right]\left\{a(\xi)\right\} \tag{12}$$

where $\{a(\xi)\}$ represents the nodal velocity potential function varying in the radial direction with respect to $\xi$. Accordingly, the velocity vector $\{v(\xi, s)\}$ can be calculated as:

$$\{\upsilon(\xi,s)\}=\left[B^1(s)\right]\{a(\xi)\}_{,\xi}+\frac{1}{\xi}\left[B^2(s)\right]\{a(\xi)\} \tag{13}$$

with

$$\begin{aligned}[B^1(s)]&=[b^1(s)][N(s)]\\ [B^2(s)]&=[b^2(s)][N(s)]_{,s}\end{aligned} \tag{14}$$

Denoting any boundary with prescribed velocity $\bar{\upsilon}_n$ in the outward normal direction *n* as $\Gamma_\upsilon$,

$$\phi_{T,n}=\bar{\upsilon}_n \text{ on } \Gamma_\upsilon, \tag{15}$$

and applying the weighted residual technique with a weighting function *w* and Green's theorem, Eq. (4) is translated into an integral equation using Eq. (15) as:

$$\int_\Omega \nabla^T w\nabla\phi^T d\Omega-\int_\Omega wk^2\phi^T d\Omega-\int_\Gamma w\bar{\upsilon}_n d\Gamma=0 \tag{16}$$

Formulating the weighting function *w* using the shape function [*N*(*s*)] as:

$$w(\xi,s)=\left[N(s)\right]w(\xi)=w(\xi)^T\left[N(s)\right]^T \tag{17}$$

and through a series of mathematical manipulations, the following expression results:

$$\begin{aligned}
&\{w(\xi_1)\}^T\left(\left[E^0\right]\xi_1\{a(\xi_1)\}_{,\xi}+\left[E^1\right]^T\{a(\xi_1)\}-\int_S\left[N(s)\right]^T\bar{\upsilon}_n(\xi_1,s)\xi_1 ds\right)\\
&-\{w(\xi_0)\}^T\left(\left[E^0\right]\xi_0\{a(\xi_0)\}_{,\xi}+\left[E^1\right]^T\{a(\xi_0)\}+\int_S\left[N(s)\right]^T\bar{\upsilon}_n(\xi_0,s)\xi_0 ds\right)\\
&-\int_{\xi_0}^{\xi_1}\{w(\xi)\}^T\begin{pmatrix}\left[E^0\right]\xi\{a(\xi)\}_{,\xi\xi}+\left(\left[E^0\right]-\left[E^1\right]+\left[E^1\right]^T\right)\{a(\xi)\}_{,\xi}\\-\left[E^2\right]\frac{1}{\xi}\{a(\xi)\}+k^2\xi\left[M^0\right]\{a(\xi)\}\end{pmatrix}d\xi=0
\end{aligned}\tag{18}$$

Eq. (18) is valid for any arbitrary $\{w(\xi)\}$, therefore, the coefficients of $\{w(\xi)\}$ should be zero, resulting in:

$$\left[E^0\right]\xi_0\{a(\xi_0)\}_{,\xi}+\left[E^1\right]^T\{a(\xi_0)\}=-\int_S\left[N(s)\right]^T\bar{\upsilon}_n(\xi_0,s)\xi_0 ds \tag{19}$$

$$\left[E^0\right]\xi_1\{a(\xi_1)\}_{,\xi}+\left[E^1\right]^T\{a(\xi_1)\}=\int_S\left[N(s)\right]^T\bar{\upsilon}_n(\xi_1,s)\xi_1 ds \tag{20}$$

$$\left[E^0\right]\xi^2\{a(\xi)\}_{,\xi\xi}+\left(\left[E^0\right]-\left[E^1\right]+\left[E^1\right]^T\right)\xi\{a(\xi)\}_{,\xi}-\left[E^2\right]\{a(\xi)\}+k^2\xi^2\left[M^0\right]\{a(\xi)\}=0 \tag{21}$$

Eqs. (19) and (20) explain the relationships between the nodal velocity potential and the integral of the velocity along boundaries $\xi_0$ and $\xi_1$, respectively. By examining the left-hand sides of these two equations, the concept of nodal flow function, denoted by $\{q(\xi)\}$, analogous to the internal nodal force function specified in Song and Wolf (1998), is introduced. The formulation of $\{q(\xi)\}$ is written as:

$$\{q(\xi)\}=\left[E^0\right]\xi\{a(\xi)\}_{,\xi}+\left[E^1\right]^T\{a(\xi)\} \tag{22}$$

Eq. (21) is the scaled boundary finite element equation corresponding to Eq. (4). It is a second-order matrix-form homogeneous ordinary differential equation (ODE) governing the variation of the nodal velocity potential function $\{a(\xi)\}$ within the domain. Only the radial variable $\xi$ appears. The other coordinate $s$ is incorporated in the coefficient matrices in the form of:

$$\begin{aligned}
\left[E^0\right] &= \int_{-1}^{1} [B^1(s)]^T [B^1(s)] |J| ds \\
\left[E^1\right] &= \int_{-1}^{1} [B^2(s)]^T [B^1(s)] |J| ds \\
\left[E^2\right] &= \int_{-1}^{1} [B^2(s)]^T [B^2(s)] |J| ds \\
\left[M^0\right] &= \int_{-1}^{1} [N(s)]^T [N(s)] |J| ds
\end{aligned} \tag{23}$$

with $|J|$ denoting the Jacobian calculated on the discretised curve $S$.

The detailed solution procedure of the scaled boundary finite element equation formulated in the frequency domain for elasto-dynamic problems has been documented in Song and Wolf (1998) within the context of solid mechanics, and has been employed by Li *et al*. (2006) with appropriate modifications to solve wave diffraction problems. Song *et al*. (2010) adopted an analogous procedure dealing with the bounded domain, but using a special function, i.e. the Hankel function as the base function to account for the Sommerfeld radiation condition when formulating the unbounded domain. Key procedures of solving Eq. (21) for the entire wave domain are reproduced in the

following subsections.

3.1.1. Bounded domain

The order of Eq. (21) is reduced from two to one at the expense of doubling the number of degrees of freedom involved in the system by introducing the following variable:

$$\{X(\xi)\} = \begin{Bmatrix} \{a(\xi)\} \\ \{q(\xi)\} \end{Bmatrix} \tag{24}$$

to incorporate the nodal velocity potential function $\{a(\xi)\}$ and the nodal flow function $\{q(\xi)\}$. Consequently, Eq. (21) is rewritten as a first-order matrix-form ordinary differential equation:

$$\bar{\xi}\{X(\bar{\xi})\}_{,\bar{\xi}} = -[Z]\{X(\bar{\xi})\} - \bar{\xi}^2[M]\{X(\bar{\xi})\} \tag{25}$$

with a newly-defined independent variable $\bar{\xi} = ka\xi$, and the Hamiltonian matrix $[Z]$ formulated by the coefficient matrices of Eq. (21) as :

$$[Z] = \begin{bmatrix} [E^0]^{-1}[E^1]^T & -[E^0]^{-1} \\ -[E^2] + [E^1][E^0]^{-1}[E^1]^T & -[E^1][E^0]^{-1} \end{bmatrix} \tag{26}$$

Matrix $[M]$ in Eq. (25) is related to the coefficient matrix $[M^0]$ as:

$$[M]=\frac{1}{a^2}\begin{bmatrix}0 & 0\\ [M^0] & 0\end{bmatrix} \tag{27}$$

Solving Eq. (25) involves a matrix decomposition of the Hamiltonian matrix [*Z*]. The Jordan's decomposition is suggested by Li *et al*. (2006) and Song *et al*. (2010):

$$[Z][T]=[T][\Lambda] \tag{28}$$

in which [*T*] is the invertible Jordan matrix; [Λ] is constructed by the eigenvalues in the form of:

$$[\Lambda]=\begin{bmatrix}[\lambda_j] & & \\ & \begin{bmatrix}0 & 1\\ 0 & 0\end{bmatrix} & \\ & & -[\lambda_j]\end{bmatrix} \tag{29}$$

where $j$ = 1, 2, …, $n$-1; $n$ is the number of degrees of freedom in Eq. (21); $\mathrm{Re}(\lambda_j) \geq 0$. Through a series of matrix manipulations, the solution of Eq. (25) is sought as:

$$\left\{X\left(\bar{\xi}\right)\right\}=[T]\left[R\left(\bar{\xi}\right)\right]\bar{\xi}^{[\Lambda]}\bar{\xi}^{[U]}\{C\} \tag{30}$$

with

$$\left[R\left(\bar{\xi}\right)\right]=[I]+\bar{\xi}^2[R_1]+\bar{\xi}^4[R_2]+\cdots+\bar{\xi}^{2m}[R_m]+\cdots \tag{31}$$

and an upper-triangular matrix [$U$] with zero diagonal entries. Introducing $\left[Y\left(\bar{\xi}\right)\right]=\bar{\xi}^{[U]}$ and $\left[K\left(\bar{\xi}\right)\right]=[T]\left[R\left(\bar{\xi}\right)\right]$ for brevity, Eq. (30) is partitioned as:

$$\left\{X\left(\bar{\xi}\right)\right\}=\begin{bmatrix}\left[K_{11}\left(\bar{\xi}\right)\right] & \left[K_{12}\left(\bar{\xi}\right)\right]\\ \left[K_{21}\left(\bar{\xi}\right)\right] & \left[K_{22}\left(\bar{\xi}\right)\right]\end{bmatrix}\begin{bmatrix}\bar{\xi}^{[\lambda_j]} & *\\ 0 & \bar{\xi}^{-[\lambda_j]}\end{bmatrix}\begin{bmatrix}\left[Y_{11}\left(\bar{\xi}\right)\right] & \left[Y_{12}\left(\bar{\xi}\right)\right]\\ 0 & \left[Y_{22}\left(\bar{\xi}\right)\right]\end{bmatrix}\begin{Bmatrix}\{C_1\}\\ \{C_2\}\end{Bmatrix} \tag{32}$$

For a bounded domain, the solution at the scaling centre where $\bar{\xi}=ka\xi=0$ must be finite, resulting in $\{C_2\} = 0$. Comparing Eq. (32) with Eq. (24) leads to:

$$\begin{aligned}\left\{a\left(\bar{\xi}\right)\right\}&=\left[A\left(\bar{\xi}\right)\right]\{C_1\}\\ \left\{q\left(\bar{\xi}\right)\right\}&=\left[Q\left(\bar{\xi}\right)\right]\{C_1\}\end{aligned} \tag{33}$$

with

$$\begin{aligned}\left[A\left(\bar{\xi}\right)\right]&=\left[K_{11}\left(\bar{\xi}\right)\right]\bar{\xi}^{[\lambda_j]}\left[Y_{11}\left(\bar{\xi}\right)\right]\\ \left[Q\left(\bar{\xi}\right)\right]&=\left[K_{21}\left(\bar{\xi}\right)\right]\bar{\xi}^{[\lambda_j]}\left[Y_{11}\left(\bar{\xi}\right)\right]\end{aligned} \tag{34}$$

Eliminating the constant vector $\{C_1\}$ from Eq. (33) yields the algebraic equation system, viz the nodal flow function -nodal velocity potential function relationship:

$$\left\{q\left(\bar{\xi}\right)\right\}=\left[H\left(\bar{\xi}\right)\right]\left\{a\left(\bar{\xi}\right)\right\} \tag{35}$$

with

$$\left[H\left(\bar{\xi}\right)\right]=\left[Q\left(\bar{\xi}\right)\right]\left[A\left(\bar{\xi}\right)\right]^{-1}=\left[K_{21}\left(\bar{\xi}\right)\right]\left[K_{11}\left(\bar{\xi}\right)\right]^{-1} \tag{36}$$

Eq. (35) is formulated individually for each bounded subdomain based on a local scaled boundary coordinate system. It is later assembled for the solution of the entire wave domain, following the same assemblage concept in FEM, which is discussed in Section 3.1.3.

3.1.2. Unbounded domain

The unbounded domain can be represented by scaling the circular envelope towards infinity as depicted in Fig. 3 (b). The radial coordinate $\xi$ equals 1 on the circular envelope and $\infty$ at infinity. Taking advantage of the geometric property of the circular envelope, Eq. (10) can be reformulated as:

$$\begin{aligned}\hat{x}\left(\xi,s\right)&=\xi R\cos\left(s/R\right)+x_0\\ \hat{y}\left(\xi,s\right)&=\xi R\sin\left(s/R\right)+y_0\end{aligned} \tag{37}$$

with $R$ being the radius of the circular envelope.

Accordingly, the following relationships for the coefficient matrices in Eq.(23) hold:

$$\begin{aligned}\left[E^0\right] &= \frac{1}{R}\int_{-1}^{1}[N(s)]^T[N(s)]ds \\ \left[E^1\right] &= 0\cdot[I] \\ \left[E^0\right]^{-1}\left[M^0\right] &= R^2[I]\end{aligned} \tag{38}$$

Eq. (21) is thus simplified as a matrix-form Bessel's differential equation:

$$\bar{\xi}^2\left\{a(\bar{\xi})\right\}_{,\bar{\xi}\bar{\xi}} + \bar{\xi}\left\{a(\bar{\xi})\right\}_{,\bar{\xi}} - \left[E^0\right]^{-1}\left[E^2\right]\left\{a(\bar{\xi})\right\} + \bar{\xi}^2\left\{a(\bar{\xi})\right\} = 0 \tag{39}$$

by redefining $\bar{\xi}$ for the unbounded domain as: $\bar{\xi} = kR\xi$.

Combining the two linearly independent solutions of the Bessel's differential equation, i.e. the Bessel functions of the first kind and the Bessel functions of the second kind, the Hankel functions of the first kind are chosen as the base functions to formulate the series solution of Eq. (39):

$$\left\{a(\bar{\xi})\right\} = \sum_{j=1}^{m} c_j H_{r_j}\left(\bar{\xi}\right)T_j \tag{40}$$

where $T_j$ are the eigenvectors of $[E^0]^{-1}[E^2]$ resulting from an eigenvalue problem:

$$\left(\left[E^0\right]^{-1}\left[E^2\right] - r_j^2[I]\right)T_j = 0 \tag{41}$$

formulated by substituting Eq. (40) into Eq. (39); $r_j^2$ are the corresponding eigenvalues. Hence, the boundary condition at infinity Eq. (20), i.e. the Sommerfeld radiation

condition Eq. (6) is satisfied automatically.

Similar to Eq. (35) for the bounded domains, the nodal flow function-nodal velocity potential function relationship for the unbounded domain is formulated by substituting Eq. (40) into Eq. (22), and noticing that $[E^1] = 0 \cdot [I]$:

$$\left\{q\left(\bar{\xi}\right)\right\} = \left[E^0\right]\bar{\xi}\left\{a\left(\bar{\xi}\right)\right\}_{,\bar{\xi}} = \left[E^0\right]\bar{\xi}\sum_{j=1}^{m} c_j H_{r_j}^{'}\left(\bar{\xi}\right)T_j \tag{42}$$

Using Eq. (40) again, Eq. (42) is rewritten as:

$$\left\{q_S^{\infty}\left(\bar{\xi}\right)\right\} = \left[H^{\infty}\left(\bar{\xi}\right)\right]\left\{a_S^{\infty}(\bar{\xi})\right\} \tag{43}$$

where,

$$\left[H^{\infty}\left(\bar{\xi}\right)\right] = \left[E^0\right]\bar{\xi}[T][H_{bh}][T]^{-1} \tag{44}$$

with $[T] = [T_1 \quad T_2 \quad \cdots \quad T_m]$

and $[H_{bh}] = diag\left[H_{r_1}^{'}\left(\bar{\xi}\right)/H_{r_1}\left(\bar{\xi}\right) \quad H_{r_2}^{'}\left(\bar{\xi}\right)/H_{r_2}\left(\bar{\xi}\right) \quad \cdots \quad H_{r_m}^{'}\left(\bar{\xi}\right)/H_{r_m}\left(\bar{\xi}\right)\right]$.

It should be made clear that the Sommerfeld radiation condition is only associated with the scattered waves. Therefore, a subscript ‘*s*’ is introduced in Eq. (43) to signify that the nodal flow function and the nodal velocity potential function are in terms of the scattered

waves only. A superscript '$\infty$' is used for the unbounded domain.

### 3.1.3. Wave domain solution

As indicated in Sections 3.1.1 and 3.1.2, each subdomain (bounded or unbounded) has an individual SBFEM formulation associated with a particular scaled boundary coordinate system. These formulations are independent, and are only effective for their own-defined domain. To solve the entire wave field, these formulations need to be assembled according to the relationships in terms of the nodal variables at the discretised interfaces between adjacent subdomains. These nodal values are then solved from the assembled equation subject to boundary conditions and the incident wave information. Subsequently, they are extracted back into each subdomain to calculate the integral constants ($\{C_1\}$ in Eq. (33) for bounded domains and $c_j$ in Eq. (40) for the unbounded domain). Afterwards, analytical nodal functions are formulated according to Eq. (33) for bounded domains or Eq. (40) for the unbounded domain. Finally, the solution of the entire wave domain can be obtained by specifying the scaled boundary coordinates $\xi$ and $s$. The subdomain assemblage process and the solution procedure are detailed as follows.

Eq. (35) is formulated on the discretised boundary for bounded subdomains $S_i$ ($i$ = 1, 2, …, 7) as:

$$\left\{q^b\right\}=\left[H^b\right]\left\{a^b\right\} \tag{45}$$

and then is assembled for the entire bounded subdomain $S_\mathrm{b}$ according to the conditions that the velocity potentials ($\phi_T$, $\phi_I$ and $\phi_S$) are continuous (Eq. (46)) at the subdomain interfaces $\Gamma_\mathrm{intf}$ (refer to Fig. 2); the flows ($q_T$, $q_I$ and $q_S$), however, hold the same magnitude but opposite signs (Eq. (47)).

$$\phi=\phi^{adj} \text{ on } \Gamma_{intf} \tag{46}$$

$$q=-q^{adj} \text{ on } \Gamma_{intf} \tag{47}$$

$\phi$ and $q$ with superscript '*adj*' refer to the velocity potential and the flow from an adjacent subdomain. Expressing the total nodal flow and the total nodal velocity potential by the sum of corresponding incident and scattered components, the assembled nodal flow-nodal velocity potential relationship for the entire bounded domain $S_\mathrm{b}$ is written as:

$$\left\{q_I^b\right\}+\left\{q_S^b\right\}=\left[H^b\right]\left(\left\{a_I^b\right\}+\left\{a_S^b\right\}\right) \tag{48}$$

In the subsequent assemblage of $S_\mathrm{b}$ and $S_\infty$, the equalities on the auxiliary circular envelope $\Gamma_\mathrm{auxi}$ are addressed. Again, the velocity potentials ($\phi_T$, $\phi_I$ and $\phi_S$) on $\Gamma_\mathrm{auxi}$ are continuous (Eq. (49)), and the flows ($q_T$, $q_I$ and $q_S$) are equal in magnitude but opposite in sign (Eq. (50)).

$$\phi^{\infty} = \phi^{adj} \text{ on } \Gamma_{auxi} \tag{49}$$

$$q^{\infty} = -q^{adj} \text{ on } \Gamma_{auxi} \tag{50}$$

As the outward normal directions of the bounded domain and the unbounded domain on the auxiliary circular envelope are opposite to each other, Eq. (43) is reformulated in conformity with Eq. (48) for assemblage purposes as:

$$\left[H^{\infty}\right]\left\{a_S^{\infty}\right\} = -\left\{q_S^{\infty}\right\} \tag{51}$$

and is subsequently added by $\left[H^{\infty}\right]\left\{a_I^{\infty}\right\}$ to both sides, which leads to:

$$\left[H^{\infty}\right]\left\{a_T^{\infty}\right\} = -\left\{q_S^{\infty}\right\} + \left[H^{\infty}\right]\left\{a_I^{\infty}\right\} \tag{52}$$

By rearranging Eq. (48) as:

$$\left[H^{\infty}\right]\left\{a_T^{b}\right\} = \left\{q_T^{b}\right\} = -\left\{q_S^{\infty}\right\} - \left\{q_I^{\infty}\right\} \tag{53}$$

and combining Eqs. (52) and (53), noticing $\left\{a_T^{\infty}\right\} = \left\{a_T^{b}\right\}$, yields:

$$\left(\left[H^{b}\right] - \left[H^{\infty}\right]\right)\left\{a_T\right\} = -\left\{q_I^{\infty}\right\} - \left[H^{\infty}\right]\left\{a_I\right\} \tag{54}$$

Eq. (54) represents the assembled nodal flow -nodal velocity potential relationship for the entire wave domain discretisation. The right-hand side of Eq. (54) is in terms of the

incident wave information, which enables the total velocity potential $\left\{a_T^b\right\}$ ($\left\{a_T^\infty\right\}=\left\{a_T^b\right\}$) of all discretised nodes to be obtained by simply solving a linear algebraic equation. Once the nodal total velocity potential $\left\{a_T^b\right\}$ for the entire discretisaion is solved, they are extracted for each individual subdomain according to the degrees of freedom involved. For each bounded subdomain $S_i$ ($i$ = 1, 2, …, 7), the constant vector $\{C_1\}$ in Eq. (33) is first determined according to the nodal value on the discretised boundary. Subsequently, $\left\{a\left(\bar{\xi}\right)\right\}$ is calculated for any specific $\xi$ (ranging from 0 to 1), and $\left\{\phi\left(\xi,s\right)\right\}$ within the subdomain can be obtained by specifying the circumferential coordinate $s$. For the unbounded domain outside the auxiliary circular envelope, as the series expression in Eq. (40) is only associated with the scattered waves, the nodal scattered velocity potential is extracted first by subtracting the incident component from the total nodal velocity potential. Afterwards, the constant $c_j$ in Eq. (40) is gained and the total velocity potential for the unbounded domain is solved by adding the incident component to the scattered counterpart at any $\xi$ (ranging from 1 to ∞) and $s$. Subsequently, other derivative physical quantities, such as the free surface elevation $\eta_\theta$ and the dynamic wave pressure $p$ acting upon pile foundations can be computed as:

$$\eta_\theta = \frac{i\omega}{g}\phi \tag{55}$$

$$p = -\rho\,\Phi_{,t} \tag{56}$$

*3.2. Structural formulation*

Piles normally have a rather large aspect ratio of height to radius. It is common to divide the entire pile into subdomains with relatively well-proportioned length in all dimensions (Fig. 4 (a)). Similar to that introduced in Section 3.1, a local three-dimensional scaled boundary coordinate system is introduced in each subdomain as shown in Fig. 4 (b). It is constituted by a scaling centre $O(x_0, y_0, z_0)$, a radial coordinate $\xi$ ranging from $\xi_0 = 0$ at $O$ to $\xi_1 = 1$ at the subdomain boundary $\Gamma$, and two coordinates $\eta$, $\zeta$ relying on the circumferential directions with their values varying over an interval of [-1, 1] for each discretised element on $\Gamma$. The scaled boundary transformation equation is therefore formulated as:

$$\begin{aligned} \hat{x}(\xi,\eta,\zeta) &= \xi\left[N(\eta,\zeta)\right]\{x\} + x_0 \\ \hat{y}(\xi,\eta,\zeta) &= \xi\left[N(\eta,\zeta)\right]\{y\} + y_0 \\ \hat{z}(\xi,\eta,\zeta) &= \xi\left[N(\eta,\zeta)\right]\{z\} + z_0 \end{aligned} \tag{57}$$

where $\{x\}$, $\{y\}$ and $\{z\}$ represent the coordinates of the discretised nodes on the subdomain surface. Eq. (57) describes the transformation from the Cartesian coordinate to the scaled boundary coordinate system with the mapping function $[N(\eta, \zeta)]$. With this geometric mapping, the differential operator $[L]$ is reformulated in the scaled boundary coordinate system using $\xi$, $\eta$ and $\zeta$ as:

$$[L]=\left[b^1(\eta,\zeta)\right]\frac{\partial}{\partial\xi}+\frac{1}{\xi}\left(\left[b^2(\eta,\zeta)\right]\frac{\partial}{\partial\eta}+\left[b^3(\eta,\zeta)\right]\frac{\partial}{\partial\zeta}\right) \tag{58}$$

in which, $[b^1(\eta, \zeta)]$, $[b^2(\eta, \zeta)]$ and $[b^3(\eta, \zeta)]$ only depend on the boundary discretisation, and are independent of the radial coordinate $\xi$.

Using the same shape function $[N(\eta, \zeta)]$ as for the boundary discretisation, the displacement amplitude is expressed as:

$$\{u(\xi,\eta,\zeta)\}=[N(\eta,\zeta)]\{u(\xi)\} \tag{59}$$

where $\{u(\xi)\}$ represents the displacement variation with the radial coordinate $\xi$. The stress and strain fields can be calculated as:

$$\begin{aligned}\{\varepsilon\}&=\{\varepsilon(\xi,\eta,\zeta)\}=\left[B^1(\eta,\zeta)\right]\{u(\xi)\}_{,\xi}+\frac{1}{\xi}\left[B^2(\eta,\zeta)\right]\{u(\xi)\}\\ \{\sigma\}&=\{\sigma(\xi,\eta,\zeta)\}=[D]\left(\left[B^1(\eta,\zeta)\right]\{u(\xi)\}_{,\xi}+\frac{1}{\xi}\left[B^2(\eta,\zeta)\right]\{u(\xi)\}\right)\end{aligned} \tag{60}$$

in which $[B^1(\eta, \zeta)]$ and $[B^2(\eta, \zeta)]$ are formulated as:

$$\begin{aligned}[B^1(\eta,\zeta)]&=[b^1(\eta,\zeta)][N(\eta,\zeta)]\\ [B^2(\eta,\zeta)]&=[b^2(\eta,\zeta)][N(\eta,\zeta)]_{,\eta}+[b^3(\eta,\zeta)][N(\eta,\zeta)]_{,\zeta}\end{aligned} \tag{61}$$

Applying the weighted residual technique and Green's theorem, and through a series of manipulations, the governing PDEs (7)-(9) are transformed into the second-order matrix-form Euler-Cauchy ODEs with respect to the nodal displacement function $\{u(\xi)\}$:

$$[E^0]\xi^2\{u(\xi)\}_{,\xi\xi}+\left(2[E^0]+[E^1]^T-[E^1]\right)\xi\{u(\xi)\}_{,\xi}+\left([E^1]^T-[E^2]\right)\{u(\xi)\}=0 \tag{62}$$

Eq. (62) is the scaled boundary finite element equation for structural behaviour analysis of the pile foundation. In Eq.(62), only the radial coordinate $\xi$ appears. The other two coordinates $\eta$ and $\zeta$ are incorporated in the coefficient matrices in the form of:

$$\begin{aligned}\left[E^0\right]&=\int_{-1}^{1}\int_{-1}^{1}[B^1(\eta,\zeta)]^T[D][B^1(\eta,\zeta)]\left|J(\eta,\zeta)\right|d\eta d\zeta\\ \left[E^1\right]&=\int_{-1}^{1}\int_{-1}^{1}[B^2(\eta,\zeta)]^T[D][B^1(\eta,\zeta)]\left|J(\eta,\zeta)\right|d\eta d\zeta\\ \left[E^2\right]&=\int_{-1}^{1}\int_{-1}^{1}[B^2(\eta,\zeta)]^T[D][B^2(\eta,\zeta)]\left|J(\eta,\zeta)\right|d\eta d\zeta\end{aligned} \tag{63}$$

where [$D$] is the elastic matrix representing the physical property of the pile foundation. The three matrices [$E^0$], [$E^1$] and [$E^2$] in Eq.(63) are first formulated for each individual element discretised on $\Gamma$ and then assembled in the same way as in FEM.

To solve the scaled boundary finite element Eq.(62), a new variable

$$\left\{X(\xi)\right\}=\begin{Bmatrix}\xi^{+0.5}\left\{u(\xi)\right\}\\ \xi^{-0.5}\left\{Q(\xi)\right\}\end{Bmatrix} \tag{64}$$

is introduced to incorporate the nodal displacement function $\{u(\xi)\}$ and the nodal force function$\{Q(\xi)\}$, which is expressed as:

$$\left\{Q(\xi)\right\}=\left[E^0\right]\xi^2\left\{u(\xi)\right\}_{,\xi}+\left[E^1\right]^T\xi\left\{u(\xi)\right\} \tag{65}$$

By introducing $\{X(\xi)\}$ and employing a Hamiltonian matrix $[Z]$, which is formulated by the coefficient matrices of Eq.(62) and the identity matrix $[I]$ as:

$$[Z]=\begin{bmatrix} \left[E^0\right]^{-1}\left[E^1\right]^T-0.5[I] & -\left[E^0\right]^{-1} \\ -\left[E^2\right]+\left[E^1\right]\left[E^0\right]^{-1}\left[E^1\right]^T & -\left[E^1\right]\left[E^0\right]^{-1}+0.5[I] \end{bmatrix} \tag{66}$$

the number of degrees of freedom of the problem is doubled, however, the order of the matrix-form ODE (62) is reduced from two to one, as can be examined from the resulting homogeneous linear ODE (67):

$$\xi\left\{X(\xi)\right\}_{,\xi}+[Z]\left\{X(\xi)\right\}=0 \tag{67}$$

The Schur decomposition has been proven to be a qualified and efficient method to solve Eq. (67). Following the solution procedure presented in Song (2004) and Li *et al.*(2010a) , The Schur decomposition of the Hamiltonian matrix $[Z]$ can be expressed as:

$$[Z][V]=[V][S]=\begin{bmatrix} [V_{11}] & [V_{12}] \\ [V_{21}] & [V_{22}] \end{bmatrix}\begin{bmatrix} [S_n] & * \\ 0 & [S_p] \end{bmatrix} \tag{68}$$

where $[V]$ is an orthogonal matrix, $[S]$ is a block upper triangular matrix with 1-by-1 and 2-by-2 blocks on the diagonal and $*$ stands for a real matrix. The solution of Eq. (67) is thus expressed as:

$$\{X(\xi)\} = \begin{bmatrix} [V_{11}] & [V_{12}] \\ [V_{21}] & [V_{22}] \end{bmatrix} \begin{bmatrix} \xi^{-[S_n]} & \\ & \xi^{-[S_p]} \end{bmatrix} \begin{Bmatrix} \{C_1\} \\ \{C_2\} \end{Bmatrix} \tag{69}$$

where $\{C_1\}$ and $\{C_2\}$ are integral constants.

Comparing Eq. (69) with Eq. (64), and considering the fact that the solution at the scaling centre where $\xi_0 = 0$ must be finite due to the bounded nature of the structural behaviour, yield:

$$\begin{aligned} \{u(\xi)\} &= \xi^{-0.5}[V_{11}]\xi^{-[S_n]}\{C_1\} \\ \{Q(\xi)\} &= \xi^{+0.5}[V_{21}]\xi^{-[S_n]}\{C_1\} \end{aligned} \tag{70}$$

Eliminating the integral constant $\{C_1\}$ from Eq. (70) and setting $\xi = 1$, lead to the nodal force-nodal displacement relationship on the discretised boundary:

$$[R] = \{Q\} = [K]\{u\} \tag{71}$$

with the static stiffness matrix [$K$] written as:

$$[K] = [V_{21}][V_{11}]^{-1} \tag{72}$$

Eq. (71) is formulated for each subdomain, and then assembled for the entire discretisation. The nodal displacement $\{u\}$ is solved from the assembled equation by enforcing prescribed boundary conditions, and is subsequently extracted back into each

subdomain to obtain the domain solutions by specifying $\xi$, $\eta$ and $\zeta$ in Eqs. (59) and (60).

*3.3. Integrated SBFEM model*

The SBFEM formulation and solution procedure are outlined in Sections 3.1 for the wave field behaviour and Section 3.2 for the pile foundation response, respectively. The wave field behaviour is solved first in the presence of pile foundations so that wave-induced forces can be applied for the subsequent structural behaviour investigation. As discussed, the SBFEM formulation of the wave field corresponds to the two-dimensional Helmholtz equation at the free surface level, whereas that of the pile foundations is addressed in three dimensions. Therefore, the wave field solutions need to be reinterpreted into three dimensions in order to be applicable to the structural response investigations. Referring back to the transformation from Eq. (1) to Eq. (4), it is consequently reasonable to combine the analytical expression Eq. (3) with the SBFEM solution to gain the three-dimensional wave field solution.

During the numerical implementation, conformity is required between the discretisation on $\Gamma_p$ (see Fig. 2) for the wave field analysis and on pile circumferences for structural analysis. Therefore, the physical quantities calculated from the two-dimensional mesh on $\Gamma_p$ (denoted by $\circ$ in Fig. 2) are matched correspondingly onto the three-dimensional pile mesh (Fig. 4(b)) according to the nodal $x$ and $y$ coordinates. Eq. (3) is programmed into

the two-dimensional SBFEM solution of the wave domain based on the nodal $z$ coordinates to restore the analytical variation of the wave field solution in the $z$ direction. Upon formulation into three dimensions, the wave field solution can then be applied to the subsequent structural behaviour investigations. A flowchart, illustrating the whole procedure from solving the wave field to analysing the structural behaviour, is shown in Fig. 5. Its feasibility and performance are demonstrated by the subsequent validation process.

It should be made clear that although the SBFEM model is formulated using a group of three cylindrical piles as an illustration, it is capable of addressing wave interaction with structures in a more general sense regardless of the attributes associated with the structures, such as the geometric configuration or the quantity and the spatial layout when multiple structures are involved. The proposed model can always be utilised following the procedure detailed in Sections 3. Separating the entire infinite wave domain into one unbounded domain and one bounded domain, the auxiliary circular envelope is recommended to be large enough to enclose all the structures. The unbounded domain outside the circular envelope is addressed in terms of the scattered wave field. The bounded domain, in which a further division into several subdomains should be considered, is formulated with respect to the total wave field. The subdivision of the

bounded domain $S_b$ behaves such that the scaling centre of each subdomain can be efficiently defined to make any position on the subdomain boundary visible from it. In this study, the subdomain division follows a well-balanced pattern rather than a completely arbitrary one, thereby each subdomain holding relatively even distances between the scaling centre and the domain boundary. The scaling centre of the unbounded domain is positioned at the centre of the circular envelope. These can be easily implemented in the pre-process to improve the efficiency of the SBFEM model.

## 4. MODEL VERIFICATION

In this validation process, the interaction of plane waves with a single pile foundation is examined. The velocity potential of incident plane waves is expressed as (Mei, 1989):

$$\Phi_I = -\frac{igA}{\omega} Z(z) e^{i\left(k_x x + k_y y - \omega t\right)} \tag{73}$$

In Eq. (73), $\omega$ represents the angular frequency of the incident plane waves; $i = \sqrt{-1}$. Other relevant parameters are listed in Table 1.

For ease of subsequent discussions, the orientation specifications of two variables, the incident wave angle $\alpha$ and the azimuth angle $\theta$ around the pile circumference are defined as shown in Fig. 6.

A two-dimensional SBFEM wave model is established as shown in Fig. 7 (a). A radius $R$ twice that of the pile radius $a$ is chosen for the auxiliary circular envelope. The bounded domain within the envelope, i.e. the annulus, is further divided into four subdomains, each having a scaling centre located at the geometric centre of the subdomain. All solid lines in Fig. 7 (a) are discretised using three-node quadratic elements as displayed in Fig. 7 (b).

The normalised free surface elevation $|\eta_\theta|/A$, defined as the ratio of the free surface elevation $|\eta_\theta|$ to the wave amplitude $A$, is calculated under the prescribed wave conditions and compared with the analytical solution (Zhu, 1993) in Fig. 8 for a finite region and in Fig. 9 around the pile circumference, respectively. The two figures demonstrate excellent performance of the wave field solution.

Subsequently, a three-dimensional model of the pile foundation is prepared for the structural behaviour analysis. Five subdomains with well-proportioned geometric dimensions are designed with the scaling centre of each subdomain coincident with the geometric centre. The surface of the pile, as well as the interfaces between adjacent subdomains is discretised using eight-node quadratic quadrilateral elements. In order for the nodal physical quantities from the wave field solution to be matched onto the pile model, a consistent discretisation scheme along the pile circumference between the two

models is required. Following the procedure outlined in Section 3.2, the displacement components in the *x*, *y* and *z* directions of the pile foundation are calculated, and those along the pile height at $\theta = 0$ are plotted in Fig. 10.

For validation purposes, the displacement components are denoted by the suffix '-*Numerical*' and compared in Fig. 10 with those calculated from the explicit wave pressure expression (Zhu, 1993), which is denoted by the suffix '-*Analytical*'. Note that in both cases, the wave pressure is evaluated up to the free surface elevation by stretching the coordinate *z* according to Wheeler's method (1969). Satisfactory agreement is achieved between the two results. Fig. 8-Fig. 10 demonstrate the credibility of the proposed model in solving wave-structure interaction problems. This model will be employed in the subsequent investigation of wave interaction with pile group foundations, which will be discussed in Part II of this study (Li et al., 2012).

## 5. CONCLUSIONS

This study employs SBFEM to investigate the integration of two contemporary debatable issues within the context of ocean engineering: the wave field behaviour in the presence of structures and the corresponding structural response when subject to resultant wave forces. Part I of this study, i.e. this paper, mainly deals with the physical and mathematical formulations. Prior to the SBFEM formulation of the wave field, the

Laplace equation governing the entire wave field is processed into the Helmholtz equation by separating the vertical-direction component from the velocity potential expression. This leads to a two-dimensional SBFEM investigation of the wave field at the free surface level. Well-planned subdomain division of the two-dimensional wave domain into one unbounded and several bounded subdomains is required so that: (1) the Sommerfeld radiation condition at infinity can be precisely satisfied by employing the Hankel function in the formulation of the unbounded domain; (2) irregular geometric configuration or complex spatial arrangement of piles can be easily dealt with. Upon assemblage, the wave domain is solved after the boundary conditions are enforced.

To incorporate the wave field results into the structural analysis, conformity of the discrestisation scheme along the pile circumference is required when constructing the SBFEM model. The wave field results are re-interpreted into three dimensions by programming the analytical attenuation function in the $z$ direction into the two-dimensional results. The proposed model is verified using wave interaction with one single pile with satisfactory performance: (1) accurately captures the boundary condition at infinity for the unbounded wave domain; (2) effectively addresses the wave-pile group interaction problem in three dimensions however with released computational burden; (3) successfully incorporates a scalar field in which the wave field behaviour is explored, and

a vector field where the structural response is investigated.

The formulation of the present study intensively focuses on the wave-structure interaction, external loads from superstructures acting on the pile groups are not considered. For guiding engineering design when a specific project is involved, these loads need to be applied in the SBFEM model, following the same way as in other analyses. Another simplification is in relation to the boundary condition at the seabed level, where pile foundations are seated and their displacements are assumed zero. The relative motion between piles and the seabed are beyond the scope of the present study. These aspects will be taken into consideration in the future investigation of the wave-structure interaction. The application of the proposed model to wave interaction with pile groups, detailing the wave field behaviour and the pile group responses, is presented as Part II of the three-dimensional investigation of wave-pile group interaction using SBFEM (Li et al., 2012).

ACKNOWLEDGEMENTS

The first author would like to thank Dr. Hao Song from Newcastle University, United Kingdom, for his technical assistance through email correspondence.

## REFERENCES

U.S. Coast Guard, 1983. "Report on Ocean Ranger". Report of U.S. Coast Guard Marine Board of

Investigation including Commandant's Action Report, Washington, D.C.

Bazyar, M.H., 2007. Dynamic soil-structure interaction analysis using the scaled boundary finite-element method. The University of New South Wales, Sydney, Australia.

Benassai, G., 2006. Introduction to coastal dynamics and shoreline protection. WIT Press, Southhampton, England.

Chatjigeorgiou, I.K., Mavrakos, S.A., 2010. An analytical approach for the solution of the hydrodynamic diffraction by arrays of elliptical cylinders. Applied Ocean Research 32 (2), 242-251.

Goda, Y., 2010. Random Seas and Design of Maritime Structures, 3rd ed. World Scientific.

Gould, P.L., 1994. Introduction to linear elasticity, 2nd ed. Springer-Verlag, New York.

Kagemoto, H., Yue, D.K.P., 1986. Interactions among Multiple 3-Dimensional Bodies in Water-Waves - an Exact Algebraic-Method. Journal of Fluid Mechanics 166, 189-209.

Kashiwagi, M., 2000. Hydrodynamic interactions among a great number of columns supporting a very large flexible structure. Journal of Fluids and Structures 14 (7), 1013-1034.

Lee, H.H., Wang, P.W., 2000. Dynamic behavior of tension-leg platform with net-cage system subjected to wave forces. Ocean Engineering 28 (2), 179-200.

Li, B.N., 2007. Extending the scaled boundary finite element method to wave diffraction problems. The University of Western Australia, Perth, Australia.

Li, B.N., Cheng, L., Deeks, A.J., Zhao, M., 2006. A semi-analytical solution method for two-dimensional Helmholtz equation. Applied Ocean Research 28 (3), 193-207.

Li, M., Guan, H., Zhang, H., Liu, J., 2012. Three-Dimensional Investigation of Wave-Pile Groups Interaction Using the Scaled Boundary Finite Element Method Part II: Application Results, Ocean Engineering, submitted

Li, M., Song, H., Guan, H., Zhang, H., 2010a. Schur decomposition in the scaled boundary finite element method in elastostatics, Proceedings of the 9th World Congress on Computational Mechanics (WCCM) and 4th Asia-Pacific Congress on Computational Mechanics 2010 (APCOM), Minisymposia - The Scaled Boundary Finite Element Method, Sydney, Australia.

Li, M., Song, H., Zhang, H., Guan, H., 2010b. Structural Response of Offshore Monopile Foundations to Ocean Wave Loads. Proceedings of the 9th ISOPE Pacific/Asia Offshore Mechanics Symposium (ISOPE PACOMS-2010), Busan, Korea, pp. 66-73.

Li, M., Zhang, H., Guan, H., 2011. Study of offshore monopile behaviour due to Ocean Waves. Ocean Engineering.

Linton, C.M., Evans, D.V., 1990. The Interaction of Waves with Arrays of Vertical Circular-Cylinders. Journal of Fluid Mechanics 215, 549-569.

Liu, J., Lin, G., FM, W., Li, J., 2010. The scaled boundary finite element method applied to Electromagnetic field problems, 9th World Congress on Computational Mechanics and 4th Asian Pacific Congress on Computational Mechanics, Sydney, Australia.

Maniar, H.D., Newman, J.N., 1997. Wave diffraction by a long array of cylinders. Journal of Fluid Mechanics 339, 309-330.

Mei, C.C., 1989. The Applied Dynamics of Ocean Surface Waves. World Scientific, Singapore.

Moan, T., 2005. Safety of Offshore structures, Singapore.

Sommerfeld, A., 1949. Partial Differential Equations in Physics. Academic Press, New York.

Song, C.M., 2004. A matrix function solution for the scaled boundary finite-element equation in statics. Computer Methods in Applied Mechanics and Engineering 193 (23-26), 2325-2356.

Song, C.M., Wolf, J.P., 1996a. Consistent infinitesimal finite-element cell method for diffusion equation in unobounded domain. Computer Methods in Applied Mechanics and Engineering 132, 16.

Song, C.M., Wolf, J.P., 1996b. Consistent infinitesimal finite-element cell method: three-dimensional vector wave equation. International Journal for Numerical Methods in Engineering 39, 20.

Song, C.M., Wolf, J.P., 1997. The scaled boundary finite-element method - Alias consistent infinitesimal finite-element cell method - For elastodynamics. Computer Methods in Applied Mechanics and Engineering 147 (3-4), 329-355.

Song, C.M., Wolf, J.P., 1998. The scaled boundary finite-element method: analytical solution in frequency domain. Computer Methods in Applied Mechanics and Engineering 164 (1-2), 249-264.

Song, H., Tao, L.B., Chakrabarti, S., 2010. Modelling of water wave interaction with multiple cylinders of arbitrary shape. Journal of Computational Physics 229 (5), 1498-1513.

Spring, B.H., Monkmeyer, P.L., 1974. Interaction of plane waves with vertical cylinders. Proceeding of 14th International Conference on Coastal Engineering (ASCE) Ch. 107, 1828-1849.

Tao, L., Song, H., Chakrabarti, S., 2009. Spacing Effect on Hydrodynamics of Two Adjacent Offshore Caissons. ASME Conference Proceedings 2009 (43444), 127-133.

Tao, L.B., Song, H., Chakrabarti, S., 2007. Scaled boundary FEM solution of short-crested wave diffraction by a vertical cylinder. Comput. Methods Appl. Mech. Engrg. 197, 232-242.

Walker, D.A.G., Eatock Taylor, R., 2005. Wave diffraction from linear arrays of cylinders. Ocean Engineering 32 (17-18), 2053-2078.

Wang, C.Z., Wu, G.X., 2007. Time domain analysis of second-order wave diffraction by an array of vertical cylinders. Journal of Fluids and Structures 23 (4), 605-631.

Wang, Y., Lin, G., Hu, Z., 2010. A Coupled FE and Scaled Boundary FE Approach for the Earthquake Response Analysis of Arch Dam-Reservoir-Foundation System, 9th World Congress on Computational Mechanics and 4th Asian Pacific Congress on Computational Mechanics, Sydney, Australia.

Wheeler, J.D., 1969. Methods for Calculating Forces Produced by Irregular Waves, Offshore Technology Conference. Offshore Technology Conference, Houston, United States of America.

Wolf, J.P., Song, C.M., 1996. Finite-element modelling of unbounded media. Wiley, Chichester.

Wu, C., Watanabe, E., Utsunomiya, T., 1995. An eigenfunction expansion-matching method for analyzing the wave-induced responses of an elastic floating plate. Applied Ocean Research 17 (5), 301-310.

Yang, Z.J., 2006. Application of scaled boundary finite element method in static and dynamic fracture problems. Acta Mechanica Sinica 22 (3), 243-256.

Yang, Z.J., Deeks, A.J., 2007. Fully-automatic modelling of cohesive crack growth using a finite element-scaled boundary finite element coupled method. Engineering Fracture Mechanics 74 (16), 2547-2573.

Yilmaz, O., Incecik, A., 1998. Analytical solutions of the diffraction problem of a group of truncated vertical cylinders. Ocean Engineering 25 (6), 385-394.

Zhao, F., Kinoshita, T., Bao, W., 2008. Wave Fields Diffracted by an Array of Truncated Circular Cylinders. ASME Conference Proceedings 2008 (48234), 399-406.

Zhu, S., 1993. Diffraction of short-crested waves around a circular cylinder. Ocean Engineering 20 (4), 389-407.

Table 1. Relevant parametric information of the validation example

| Parameters | | Notations | Magnitudes | Units |
|---|---|---|---|---|
| Pile parameters | Pile radius | $a$ | 1 | m |
| | Pile height | $h$ | 10 | m |
| | Young's modulus | $E$ | $2.8\times10^{10}$ | Pa |
| | Possion's ratio | $v$ | 0.25 | - |
| Wave parameters | Water depth | $d$ | 7.5 | m |
| | Incident wave angle | $\alpha$ | 0 | rad |
| | Wave number | $k$ | 0.1 | $m^{-1}$ |
| | Water density | $\rho$ | 1000 | $kg/m^3$ |
| | Wave amplitude | $A$ | 0.5 | m |
| Gravitational acceleration | | $g$ | 9.81 | $m/s^2$ |

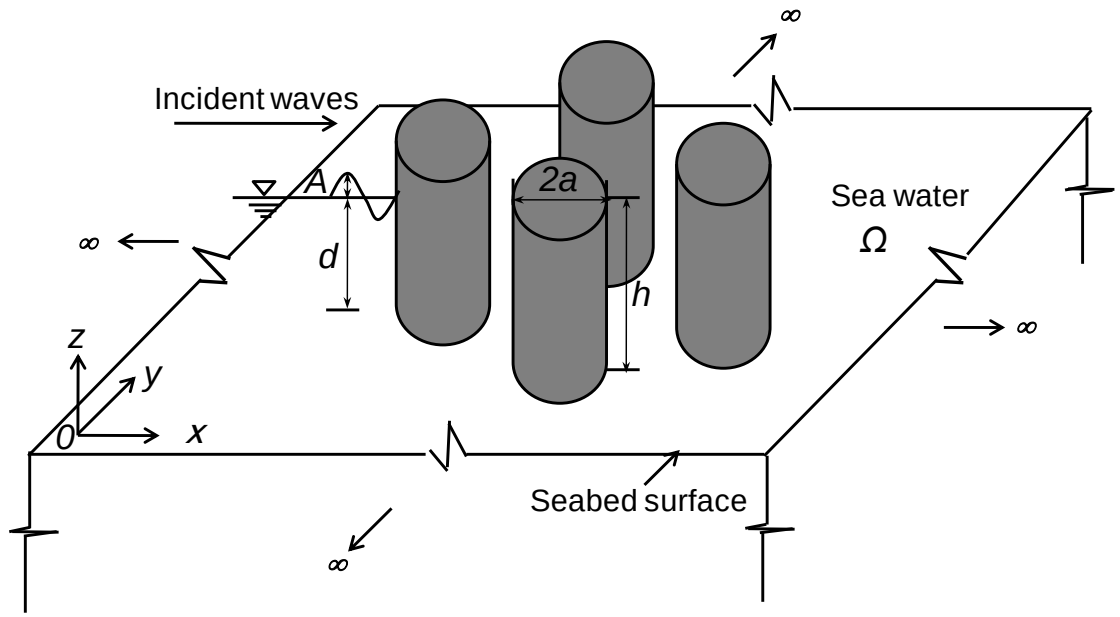


Fig. 1. Illustration of a pile group foundation in ocean environment

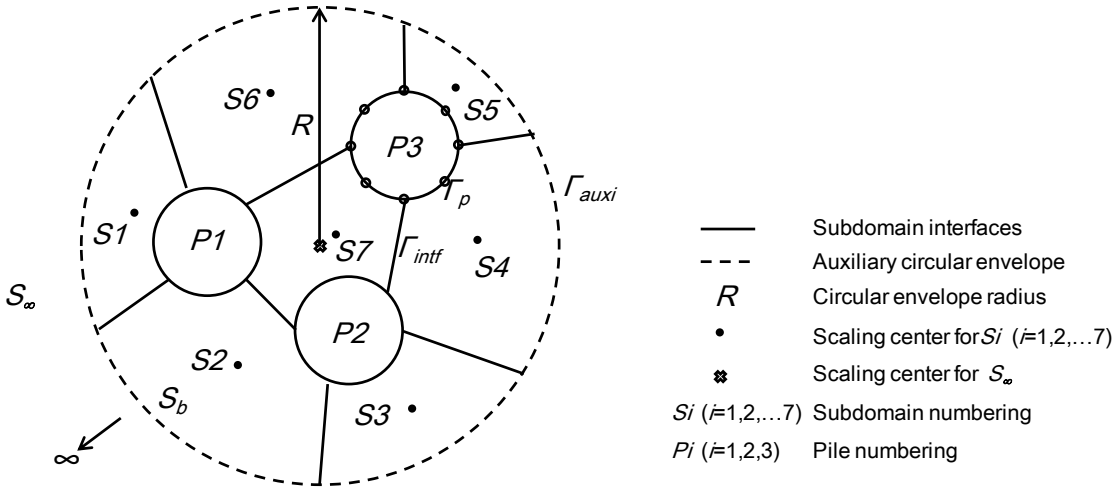


Fig. 2. Illustration of SBFEM subdomain division

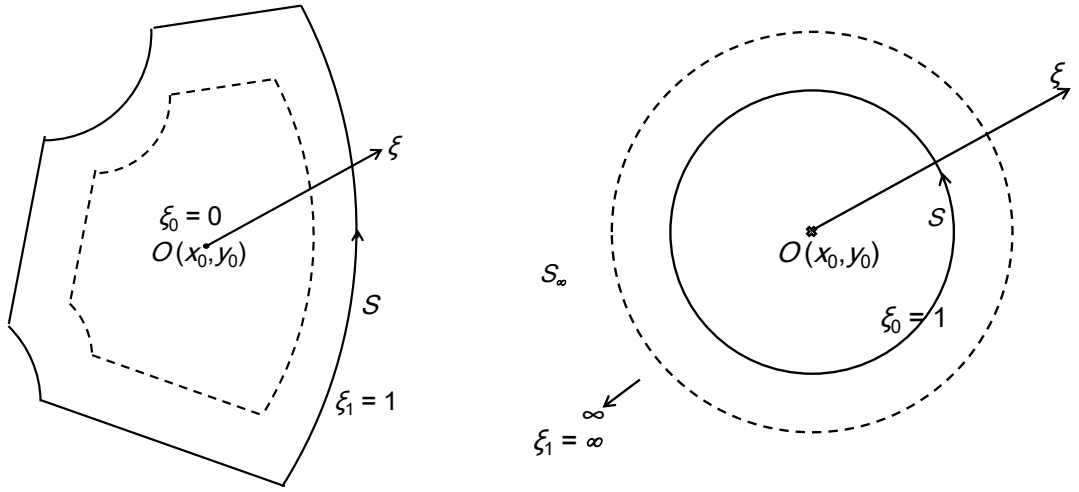


(a) (b)

Fig. 3. Illustration of the scaled boundary coordinate system: (a) bounded domain and (b) unbounded domain

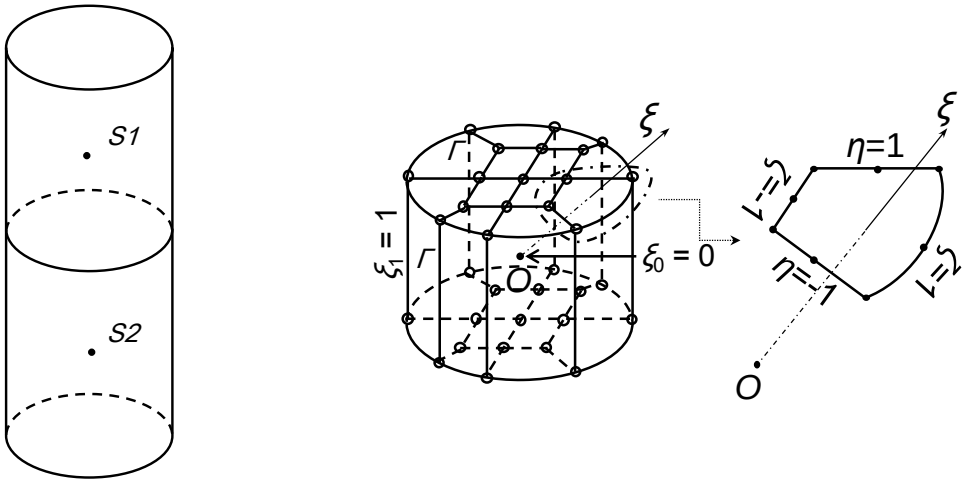


(a) (b)

Fig. 4. SBFEM model of a pile foundation: (a) subdomain division and (b) boundary discretisation

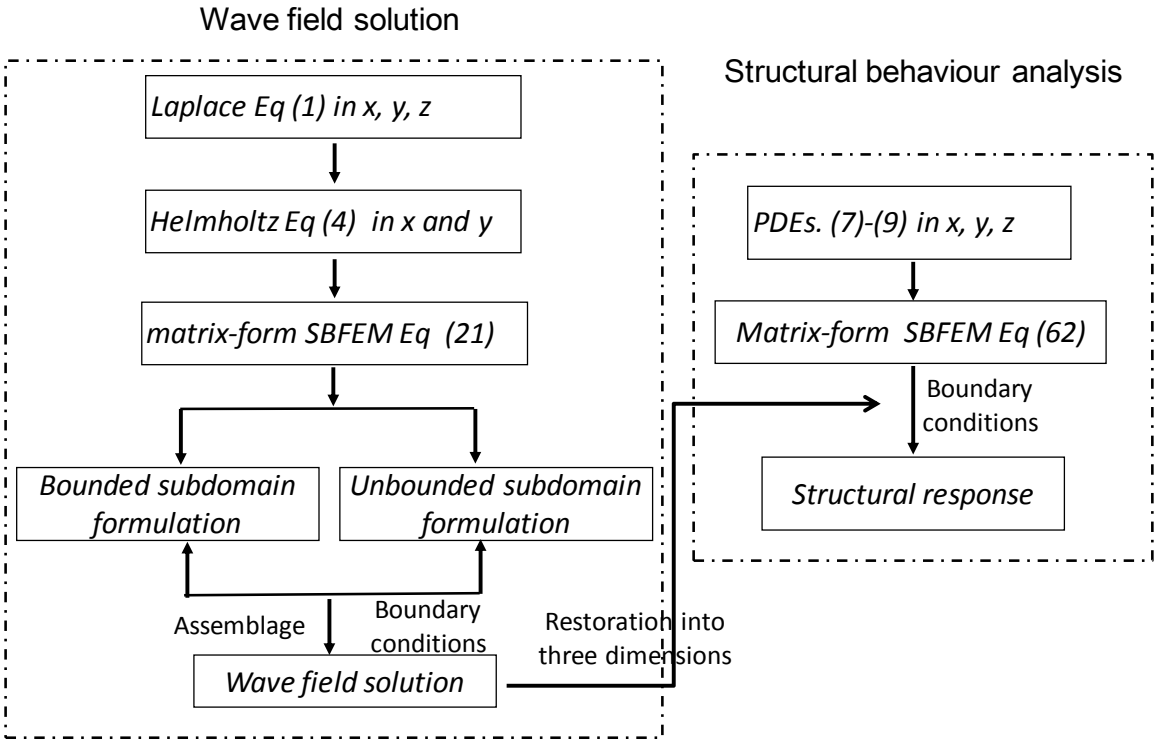


Fig. 5. Integration of wave field solution and structure behaviour analysis

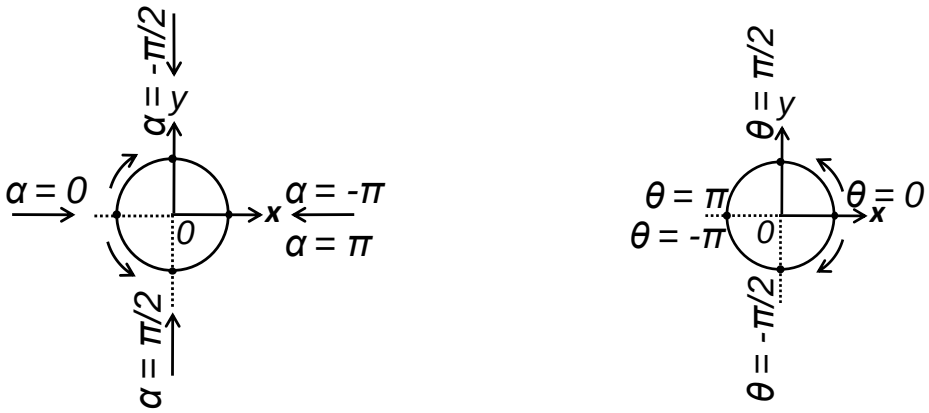


(a) (b)

Fig. 6. Reference systems of: (a) the incident wave angle $\alpha$ and (b) the azimuth angle $\theta$ around pile circumference

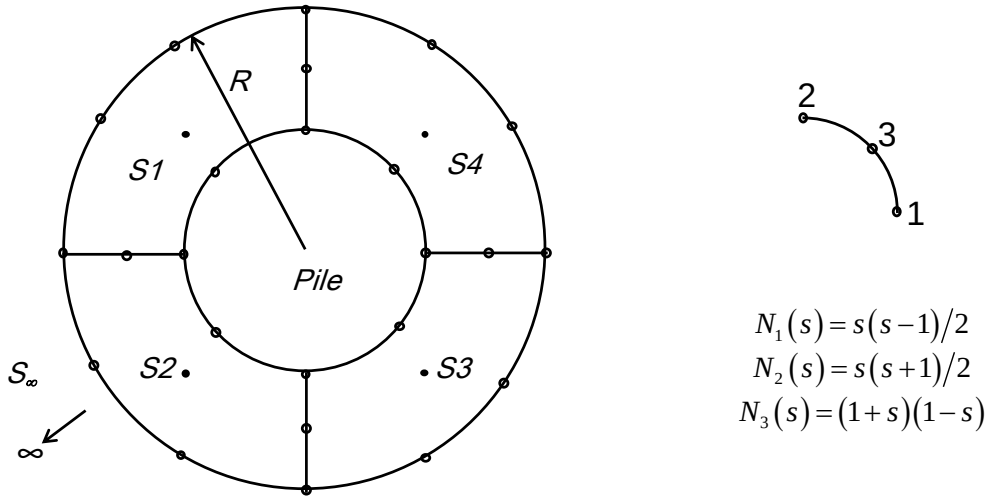


(a) (b)

Fig. 7. Two-dimensional SBFEM model for wave domain solution: (a) subdomain division and (b) scaled boundary element

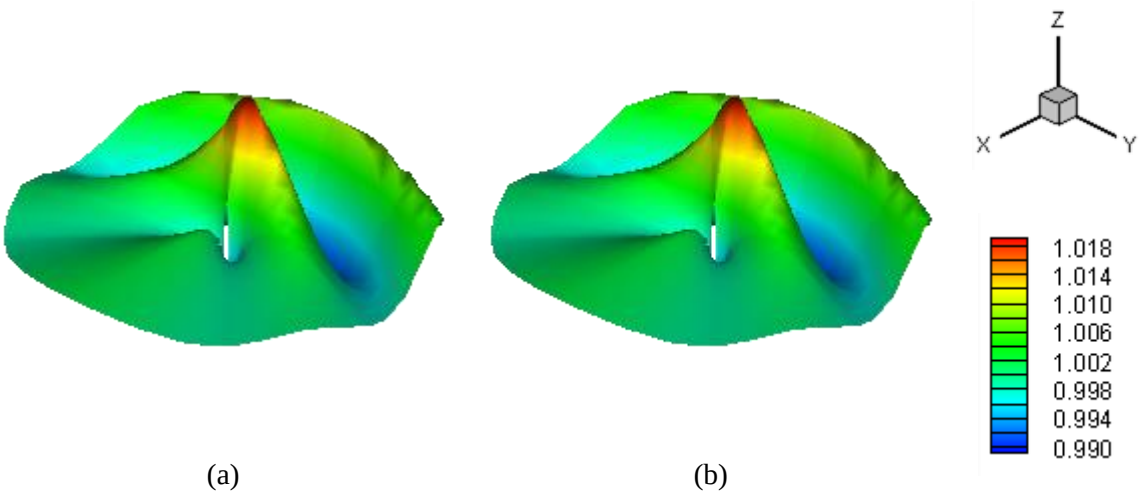


(a) (b)

Fig. 8. $|\eta_\theta|/A$ of a finite region of the wave field for plane waves ($k$ = 0.10 m$^{-1}$ and $\alpha$ = 0) interaction with a cylindrical pile from (a) analytical expression and (b) numerical calculation

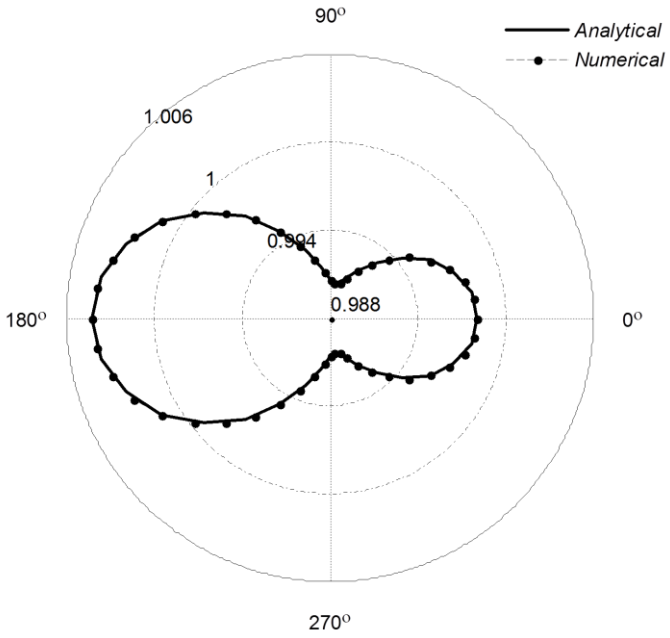


Fig. 9. Comparison of normalised free surface elevation $|\eta_\theta|/A$ around pile circumference

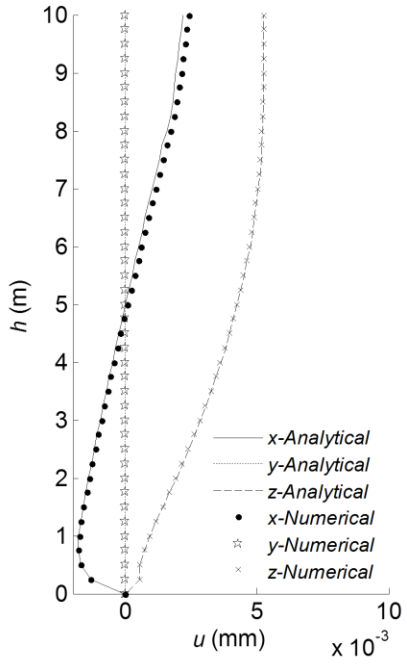


Fig. 10. Displacement comparison of the validation example